Passive and Active Neutron Matrix Correction for Heterogeneous Distributions Utilizing the Neutron Imaging Technique - 8253

Marcel F. Villani, Stephen Croft
Canberra Industries, Inc.
800 Research Parkway, Meriden, CT 06450, USA

Eloisa Alvarez, Colin G. Wilkins, Dave Stamp, John Fisher
Canberra Harwell, Ltd.
Didcot, UK

Alessandro Ambrifi, Gianluca Simone
Nucleco SpA
Casaccia, IT

Ludovic C. Bourva
International Atomic Energy Agency
Department of Safeguards
Vienna, AU

ABSTRACT

Classical Non-Destructive Assay (NDA) Passive Neutron Coincidence Counting (PNCC) and Differential Die-Away (DDA) active neutron interrogation techniques [1, 2] are well suited for determining the gross matrix correction factors for homogenous mass distributions of Special Nuclear Material (SNM) within an interfering waste drum matrix. These measured passive and active matrix correction factors are crucial in quantifying the SNM mass, associated Total Measurement Uncertainty (TMU), and Minimum Detectable Activity (MDA) within the drum. When heterogeneous SNM mass distributions are encountered, the measured SNM mass, TMU and MDA biases introduced may be 100%, or greater, especially for dense hydrogenous matrices. The standard matrix correction factors can be adjusted if a coarse spatial image of the SNM mass, relative to the matrix, is available. The image can then be analyzed to determine the spatially-adjusted, matrix correction factors case by case. This image analysis approach was accomplished by modifying the standard Passive-Active Neutron (PAN) counter design [3] to accommodate a unique data acquisition architecture that supports a newly developed image acquisition and analysis application called the Neutron Imaging Technique (NIT). The NIT functionality supports both PNCC and DDA acquisition and analysis modes and exploits the symmetry between a stored set of factory acquired NIT images with those from the unknown PAN assay. The NIT result is then an adjustment to the classical correction factor reducing, if not removing, the SNM mass bias and revealing the true TMU and MDA values. In this paper we describe the NIT for the PAN design from the software and algorithmic perspectives and how this technique accommodates waste matrix drums that are difficult, from the classical standpoint, if not impossible, to extract meaningful SNM mass, TMU and MDA results.

INTRODUCTION

Classical passive and active neutron (PAN) waste assay systems [1, 2] incorporate matrix correction techniques which strictly assume uniform SNM mass distributions within an

interfering matrix. Such correction factors are called volume average correction factors. Assays with highly hydrogenous matrix materials can lead to recoveries of less than a few percent to several hundred percent depending on pessimistic, *i.e.*, less than the volume average, or optimistic, *i.e.*, greater than the volume average, SNM mass distributions. Improvements for non-uniform SNM distributions has been previously achieved utilizing other neutron image producing techniques [4, 5, 6, 7]. The previously published techniques generally rely on low-statistic high coincidence level rates, spatial efficiency calibrations and/or image reconstruction similar to computed tomography. The Neutron Imaging Technique (NIT), the topic of this paper, only relies on a set of stored patterns, or images, each with an associated correction factor beyond the classical volume average correction factor.

PANWAS

The passive active neutron waste assay (PANWAS) system installed at the Nucleco facility in Casaccia, Italy, is described in detail elsewhere [3, 8] and fully supports the NIT. The PANWAS counter utilizes the NIT by recording the spatial passive and active matrix dependent responses for passive, and active, singles counting during the calibration phase. A pattern recognition methodology was developed for comparing the recorded responses with respect to the unknown assay measured response to determine the necessary spatial matrix correction factor depending on the degree of SNM mass non-uniformity.

The PANWAS system comprises of 9 neutron detector banks in total arranged 3 banks on a side with 3 sides of the counter populated with banks as shown in Figure 1. There are no detector banks on the roof or floor of the counter as well as the wall facing the door due to the placement of the neutron generator. The detectors are configured in a horizontal manner to provide vertical sensitivity to SNM distributions. To attain azimuthal sensitivity the drum is rotated in discrete index intervals (60^o) or dwell positions. The two degrees of freedom and three neutron detector populated walls contribute to the NIT.

All nine of the detector packages are fast neutron detector packages and can be utilized for passive and active neutron imaging input. As the drum is indexed the Singles counting data is acquired in multi-channel scaler (MCS) format utilizing the 12 Multiport-II (MPT-II) as shown in Figure 2. Nine of the 12 Multiport-II inputs are the 9 fast detector packages. The remaining three are the barrel flux monitor, cavity flux monitor and summed fast neutron detector packages.

The 9 detector packages are saved for every index position for both passive and active assays. The cavity flux monitor and barrel flux monitor are saved for every index position (60^o) for only active assays. The summed MCS data is only saved for the entire assay, *i.e.*, one full drum rotation.

Neutron Imaging Technique

The PANWAS acquisition architecture is conducive to a pattern recognition content-addressable memory imaging technique. The content-addressable imaging technique does not involve calculating spatially adjusted efficiencies or computed tomography but merely compares the content-addressable image measured with those stored in a persistent manner. The process involves the image calibration and a comparison (pattern recognition) engine. The image

calibration is tedious since the calibration, in theory, must be performed for all matrix types and potential SNM source position engaged. In particular, for the PANWAS, the image calibration must also accommodate 400 liter drum configurations which may contain three, formerly 200 liter, compacted drums of which each may contain different matrix types. By measuring all possible matrix/container configurations the NIT effectively captures the elusive, unknown, and very complex matrix dependent spatial efficiency.

The NIT involves three distinct functionalities. The first involves a database schema to store the calibration images, image correction factors and a set of C++ classes that provided high-speed access to the database. The second functionality was to design and implement a set of algorithms to map the measured image to the calibration, *i.e.*, effectively performing the content addressable memory map. The third functionality corresponds to the application of the NIT correction factors in both active and passive mode.

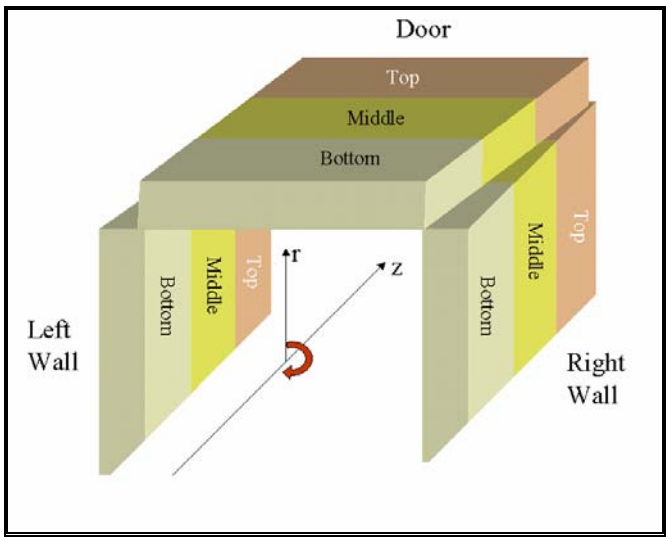

Figure 1 Physical detector layout for the PANWAS system.

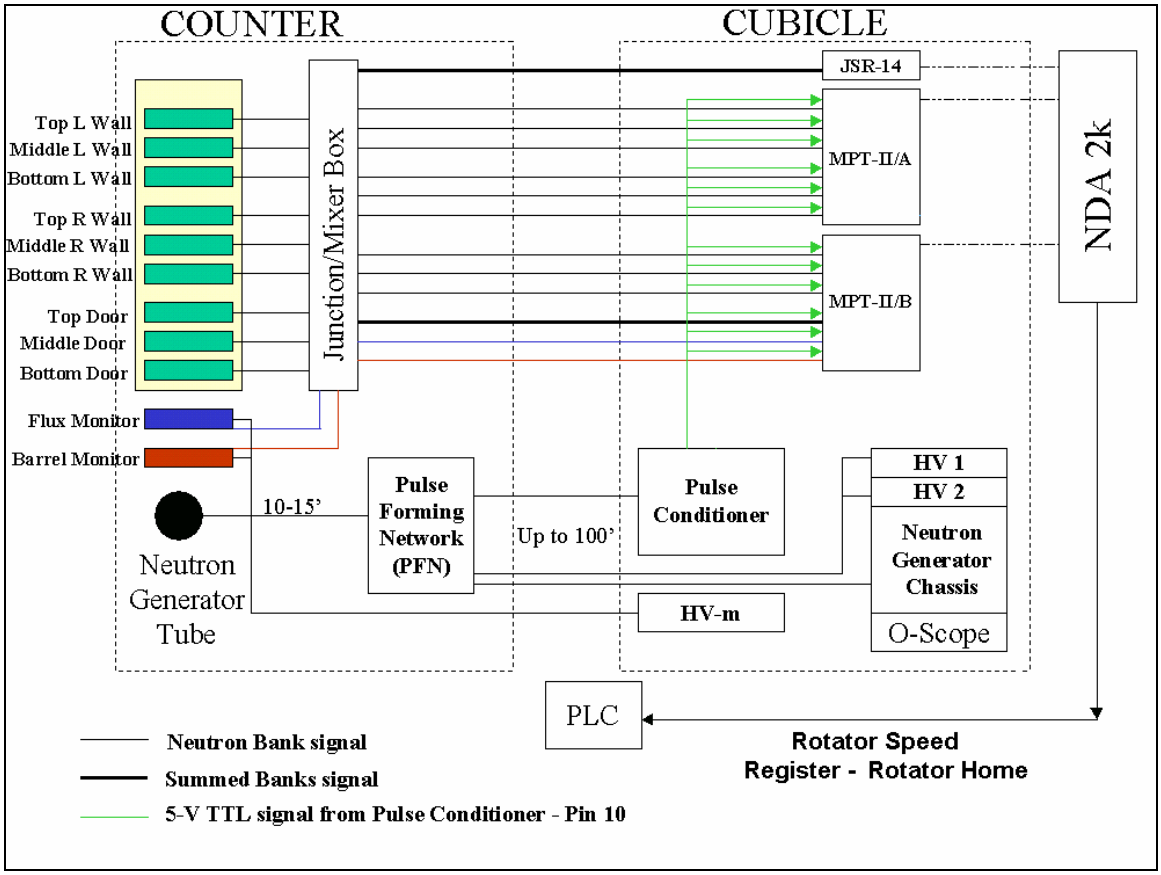

Figure 2 Electronic schematic of the PANWAS system.

Matrix Configurations

The calibration matrix elements consisted of 200L and 400L drums:

- 8 different 200 liter drums containing the following matrices: air, polyurethane, DAW (diverse active waste composed of low density material), neoprene, low and medium density wood (wood chip, glue and melinex), metallic and cemented.
- 2 different 400 liter drums, one of them empty and the other one cemented
- 2 empty 400 liter drums, one with a grouted liner, to accept the various possible combinations of simulated pucks made up of material ranging from low density (neoprene), medium density fiberboard (MDF) to high density (metallic).

Table I shows a list of the different matrix materials with approximate chemical composition.

Each calibration drum contains a self-centering frame to allow the insertion of calibration sources at different radial positions and different heights within the matrix inside the drum. Two of the frames (200 liter drums air and DAW matrices) were provided by CANBERRA Harwell Ltd. In plan view the frames are made of three or four bars (arranged like spokes on a wheel) joined at

the centre on the perimeter of a centrally located sources insertion tube. The other source insertion tubes are mounted off the spokes. There are 6 different types of frames. Figure 3 shows the plan view of the frame types i, ii and vi that correspond to the 200 liter drums and Figure 4 shows the plan view for the 400 liter drums frames, types iii, iv and v. In some of the frames there are more insertion tubes than positions used for calibration. The insertion tubes that were used in the measurements for each of the frame types were selected on the basis of establishing a similar set of measurement positions for each drum type. This provides for a self consistent analysis. Table II lists the insertion tubes that were used during the calibration and characterization measurements.

Each frame is fitted into the drum before filling and the calibration matrix is filled to surround the frame. Table III shows the main characteristics of the drums together with the corresponding matrix and frame type.

Table I Matrix materials composition.

Matrix	Description
Polyurethane	Polymer from urethane ($NH_2CO_2C_2H_5$)
Neoprene	Polymer from chloroprene ($CH_2C(Cl)CHCH_2$)
DAW	Mixed waste containing mainly paper and some plastic. We assume that the composition can be approximated by 90% wt cellulose ($C_6H_{10}O_5$) and 10% wt PVC (polyvinyl chloride, C_2H_3Cl)
Cemented	Composition assumed as SiO_2
Metallic	Mild steel
Wood	Cellulose ($C_6H_{10}O_5$) and lignum

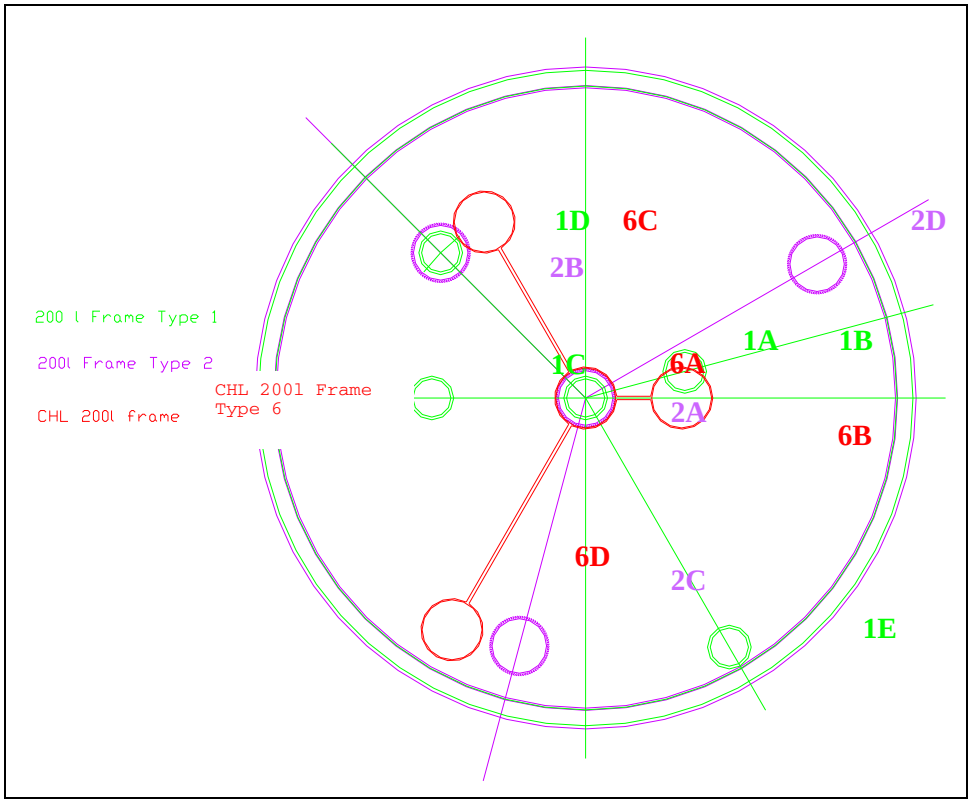

Figure 3 Plan view of the 200 litre drums frame types.

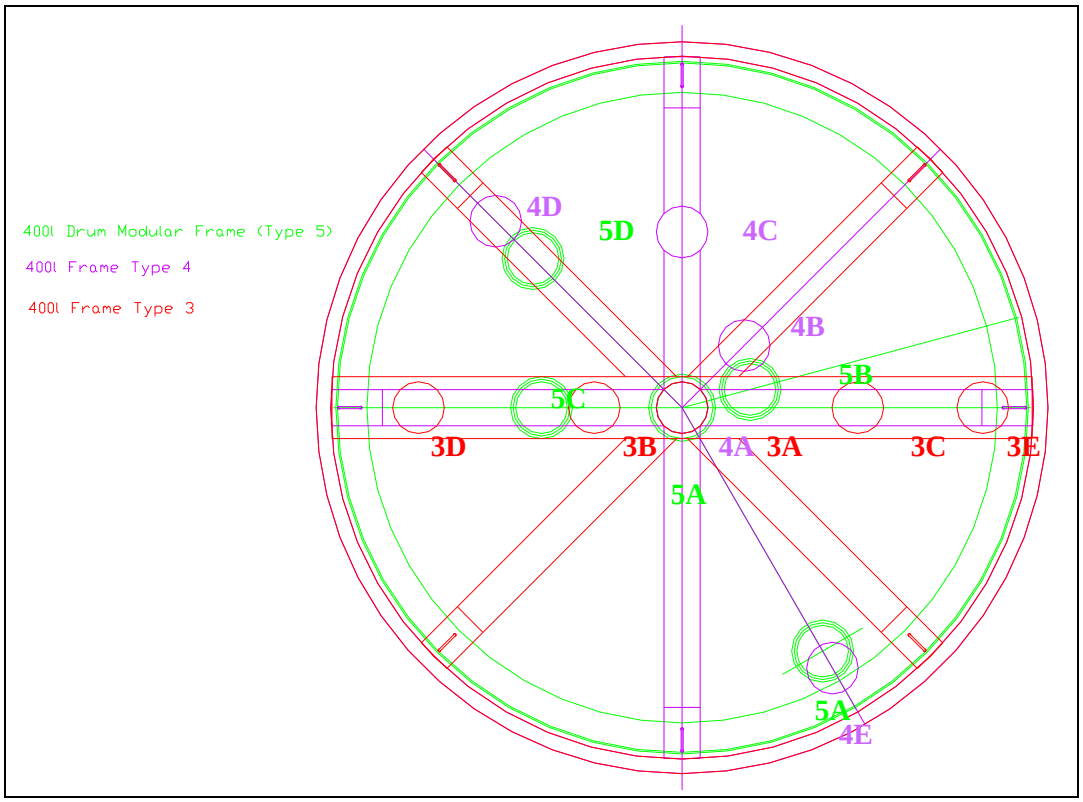

Figure 4 Plan view of the 400 litre drums and puck carrier frame types.

Table II Insertion tubes selected for calibration.

200 l Drums Frame type	Tubes identification	Approximate Distance from centre (cm)	Use for calibration
	A	0	Yes
	B	9.2	Yes
1	C	14	No
	D	16.8	Yes
	E	26.4	Yes
	A	0	Yes
2	B	16.8	Yes
	C	23.6	No
	D	24.4	Yes
	A	0	Yes
6	B	9.0	Yes
	C	18.5	Yes
	D	24.5	Yes
400 l Drums Frame type	**Tubes identification**	**Approximate Distance from centre (cm)**	**Use for calibration**
	A	0	Yes
	B	6.4	Yes
5	C	13.6	Yes
	D	20.4	No
	E	27.2	Yes
	A	0	Yes
	B	8.4	Yes
4	C	16.8	Yes
	D	25.6	No
	E	29.2	Yes
	A	0	Yes
	B	8.4	Yes
3	C	16.8	Yes
	D	25.6	No
	E	29.2	Yes

Table III Drums, matrices and frames description list (*Package density and weight depend on combination of pucks used).

Drum identification	Matrix	Gross Weight [kg]	Tare [kg]	Net Weight [kg]	Container Volume [l]	Matrix Volume [l]	Matrix Density [kg/l]	Package Density [kg/l]	Frame tubes dia [mm]	Frame Type
N220SPLmAIR01	Air	17	17	0	217.5	216	0.00129	0.00129		6
N220SPLmPUR03	Polyurethane	21	17	4	217.5	216	0.019	0.018	40	1
N220SPLmETG13	DAW	46.2	17	29.2	217.5	195	0.150	0.134		6
N220SPLmNEO04	Neoprene	113.8	17	96.8	217.5	213	0.454	0.445	40	1
N220SPlmWDL05	Wood (low density)	100.5	17	83.5	217.5	216	0.387	0.384	40	1
N220SPlmWDH06	Wood (high density)	170.5	17	153.5	217.5	215	0.714	0.706	40	1
N220SPHmMET09	Metallic	296.5	17	279.5	217.5	179	1.561	1.285	50	2
N220SPHmCEM08	Cemented	453.5	17	436.5	217.5	207	2.109	2.007	50	2
N400SPLmAIR10	Air	58	58		377	377	0.00129	0.00129	40	3
N400SPHmCEM12	Cemented	800	58	742	377	363	2.044	1.968	50	4
N400SPUcSPC14	Super-compacted unconditioned*	160 - 610	58	100-550	377	270	0.5 - 2.0	0.5 - 2.0	60	5
N2400SPCoSPC13	Super-compacted conditioned*	355 - 810	235	100-550	377	270	0.5 - 2.0	0.5 - 2.0	60	5

IMAGE CALIBRATION

The PANWAS was image calibrated for the container/matrix configurations shown in Table III with the corresponding volume weighted average correction factors depicted in Table IV. The volume weighted correction factors were obtained by measuring a several gram plutonium source for the matrix drum configurations in Table III and source positions shown in Table II. The correction factors in Table IV identify the drum to the system when extracting the image information.

Table IV. Container/matrix types and associated volume weighted matrix correction factors.

Container/Matrix	Active Matrix CF	Passive Matrix CF
N220PHmCEM08	10.107	4.186
N220SPHmMET09	3.030	1.194
N220SPLmETG13	2.430	1.163
N220SPLmNEO04	9.650	3.076
N220SPLmPUR03	1.256	1.042
N220SPLmWDH06	11.345	4.753
N220SPLmWDL05	4.318	2.856
N400SPC14 3xwood	8.991	5.054
N400SPC14 m/m/n	5.027	1.390
N400SPC14 w/n/n	5.624	3.364
N400SPHmCEM12	11.812	8.784
SPUcSPC13 m/m/n	19.046	2.822
SPUcSPC13 w/n/n	16.215	6.101
SPUcSPC13 wood	15.231	8.938
SPUcSPC13_3xtyp	4.982	6.093

KdP Correction Factor

The *KdP* correction factor is calculated from the weighted cylindrical volume elements, *CVE*. A *CVE* is defined by a calibration source position, *k*, within the matrix. The *KdP* correction factor, CF_{KdP}, is defined as,

$$CF_{NIT(srcpos)} = \frac{R_{sum\_VWA}}{R_{sum(srcpos)}} \quad \textbf{1}$$

Where the sum and volume weighted average rates are defined as,

$$R_{sum\_VWA} = \sum_{srcpos=1}^{num\_srcpos} w_{srcpos} \cdot R_{sum(srcpos)} \quad \textbf{2}$$

In the passive case, the $R_{sum(k)}$ are the environmental background subtracted Singles rates. For active assays, the $R_{sum(k)}$ are the interrogating background subtracted Singles rates.

The uncertainty in the KdP correction factor is,

$$\sigma_{CF_{KdP(k)}} = CF_{KdP(k)} \cdot \sqrt{\frac{\sigma^2_{R_{sum\_VWA}}}{R^2_{sum\_VWA}} + \frac{\sigma^2_{R_{sum(k)}}}{R^2_{sum_{(k)}}}} \quad \textbf{3}$$

Where the uncertainty in the volume weighted rates is given as,

$$\sigma_{R_{sum\_VWA}} = \sqrt{\sum_{k=0}^{srcpos-1} w_k^{\,2} \cdot \sigma^2_{R_{sum(k)}}} \quad \textbf{4}$$

Database

As each source position is added the CF_{KdP} is recalculated and stored in the high-speed access database schema as shown in Figure 5. The schema also stores other relevant information such as the source position, active gate definition, dwell positions, geometry, sample type, matrix type, density, volume, etc. The dwell positions and geometry are key fields since the image is most dependent on these variables. A set of C++ classes provides the high-speed access to the calibration and engine applications.

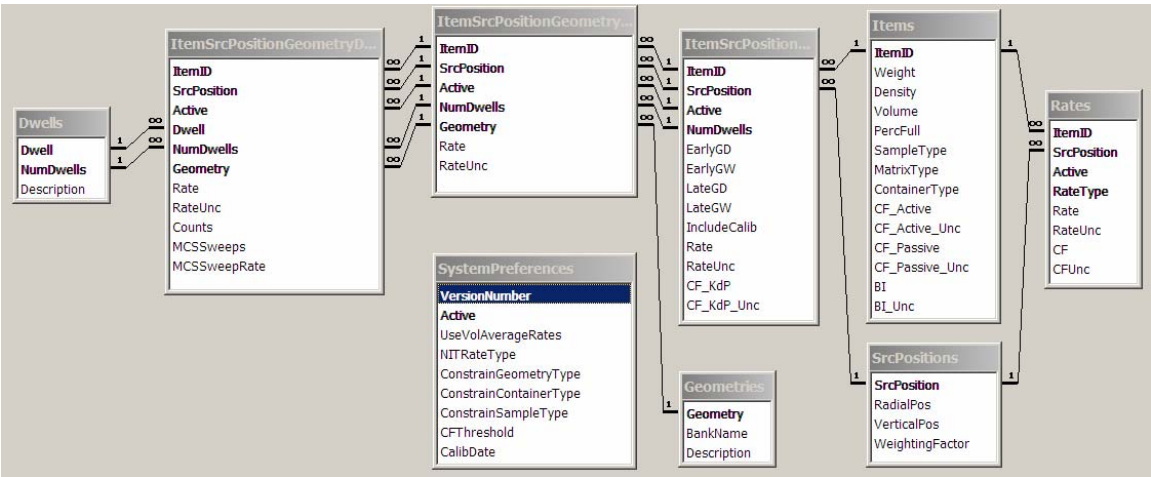

Figure 5 NIT Database schema.

IMAGE ENGINE

The image engine utilizes the calibration database and assay results to determine the image correction factor, called CF_{KdP}, for the assay. This is accomplished by implementing the NIT algorithm which involves pattern recognition utilizing a content addressable memory algorithm.

Algorithm

The engine performs two main functions; image mapping and determination of the *KdP* correction factor.

The image mapping is accomplished by calculating the *KdP* value each mapped image associated with a matrix correction factor, $CF_{passive}$ and CF_{active}, closest to the value obtained for the assay.

Define detector groups $k = 1, \ldots, p$. For a given source position, l, the measurement corrected rates, $<R>$, for group k is defined as,

$$ {}^{l}< R_{ij} >_{k} \qquad \mathbf{5}$$

Where $i = 1, \ldots, m_p$ (banks) and $j = 1, \ldots, n$ (dwells). In the case of the PANWAS counter $m_p = 3$ (Front, Right, Left) and $p = 3$ (Bottom, Middle, Top).

The passive measurement corrected rates can be obtained by directly subtracting the corresponding environmental background for the appropriate detector bank. The active measurement corrected rates are determined by subtracting a fraction, $1/(m_p*p)$ of the summed interrogating background. This is done since the interrogating background is a complicated function of the summed detector group and was not parameterized per detection group.

We define the standard deviation with respect to the radial average, *i.e.*, over dwells, as,

$$ {}^{l}\langle \sigma_i \rangle_k = \sqrt{\frac{n \cdot \sum_{j=1}^{n} {}^{l}\langle R_{ij} \rangle_k^2 - \left(\sum_{j=1}^{n} {}^{l}\langle R_{ij} \rangle_k \right)^2}{n(n-1)}} \quad \textbf{6} $$

Define the standard deviation vector as,

$$ {}^{l}\langle \sigma \rangle_k = \frac{1}{m_p} \sum_{i}^{m_p} {}^{l}\langle \sigma_i \rangle_k \quad \textbf{7} $$

With the calibration in place an assay is performed with the source in an unknown (*assay*) position. The KdP for the assay with respect to the source position *l* is then defined as,

$$ {}^{assay,l}KdP = \sum_{k=1}^{p} \left({}^{assay}\langle \sigma \rangle_k - {}^{l}\langle \sigma \rangle_k \right)^2 \quad \textbf{8} $$

The engine then persistently stores the *KdP* value and associate correction factor.

The determination of the final *KdP* correction factor applied is determined by user selectable processing and analysis control. The first processing is to determine the confidence in the counting statistics and the level of non-uniformity filter. The second stage of processing determines the actual *KdP* correction factor.

To detect if the *KdP* correction factor will be statistically viable, the SNM mass, as determined from the appropriate algorithm, passive or active, is subjected to an appropriate statistical test.

For active assays the test compares the matrix corrected equivalent mass, m_{active}, with the associated uncertainty,

$$ m_{active} > 2.4 \cdot \sigma_{m_{active}} \quad \textbf{9} $$

In the passive case, the coincidence rate, $D_{passive}$, is compared to the associated uncertainty.

$$ D_{passive} > 2.4 \cdot \sigma_{D_{passive}} \quad \textbf{10} $$

If the condition in **Eq. 9** is not met then the active NIT correction factor, CF_{NIT_Active}, is set to unity with zero associated uncertainty. Similarly, for the passive assay, if the condition in Eq. 10 is not satisfied then the associated NIT correction factor, $CF_{NIT\_Passive}$, is forced to unity with zero uncertainty.

The purpose of the non-uniformity detection algorithm is to remove the application of the NIT correction factors, passive or active, when acceptable counting statistics are engaged, *i.e.*, **Eq. 9** or **Eq. 10** are satisfied, and uniform SNM distribution conditions are observed. The test requires that for a given side of the counter the difference between the maximum and minimum rates is

greater than 3 times the corresponding maximum uncertainty for a given detector bank. This is accomplished by determining the maximum and minimum rates for all detector banks for all sides of the counter,

$$R_{\max(i,k)} = \max(^{assay} < R_{ij} >_k)$$
$$R_{\min(i,k)} = \min(^{assay} < R_{ij} >_k) \quad \textbf{11}$$

For the associated maximum and minimum rates determine the maximum uncertainty,

$$\sigma_{\max(i,k)} = \max(\sigma_{\max(i,k)}, \sigma_{\min(i,k)}) \quad \textbf{12}$$

For a given side, *i*, if all of the horizontal detector banks, *j*, pass the following test,

$$R_{\max(i,k)} - R_{\min(i,k)} > 3.0 \cdot \sigma_{\max(i)} \quad \textbf{13}$$

Then the assay is considered as a non-uniform SNM distribution. If, for all sides of the counter the condition in **Eq. 13** is not satisfied then the SNM distribution is considered as non-uniform and the associated NIT correction factors are set to unity with zero uncertainty.

Applying the NIT CF

For passive assays the NIT CF is not applied directly to final mass result. Instead, the result needs to be applied to the measurement corrected rates. Since the NIT CF is a Singles rate correction factor then the measurement corrected Doubles, D_{MC}, and Triples, T_{MC}, rates are corrected using powers of the NIT CF, *i.e.*,

$$S = S_{MC} \cdot CF_{NIT\_Passive}$$
$$D = D_{MC} \cdot CF^2_{NIT\_Passive}$$
$$T = T_{MC} \cdot CF^3_{NIT\_Passive} \quad \textbf{14}$$

$$MDA_{Passive\_coinc} = MDA_{Passive\_coinc\_unc} \cdot CF^2_{NIT\_Passive} \quad \textbf{15}$$

$$m_{active} = m_{active\_matrix} \cdot CF_{NIT\_Active}$$
$$\sigma^2_{active} = m^2_{active} \cdot \left(\frac{\sigma^2_{active}}{m^2_{active\_matrix}} + \frac{\sigma^2_{NIT\_Active}}{CF^2_{NIT\_Active}} \right) \quad \textbf{16}$$

$$MDA_{Active} = MDA_{Active\_uncorr} \cdot CF_{NIT\_Active} \quad \textbf{17}$$

This results in a proper characterization of the MDA and TMU. Generally speaking the TMU components are reduced when the NIT correction factors are applied. This can be effectively accomplished by simply "turning off" the TMU contribution when non-uniform SNM distributions are engaged.

RESULTS

An example of the door responses are shown in Figure 6 and Figure 7 for the active and passive cases respectively for the neoprene matrix. The sigma vectors, **Eq. 7**, for combustible (ETG) are shown in Table V for passive and Table VI for active. Similarly, the passive and active sigma matrices for high-density wood (WHD) and neoprene (NEO) are shown in Table VII, Table VIII, Table IX, and Table X respectively. *h1* is the bottom vertical position, *h2* is the middle and *h3* the top. *r1* is the drum radial center with *r2*, *r3*, and *r4* defined in Table II.

From Figure 6 and Figure 7 we can see that for singles counting there is a significant change in the singles rate as the drum is rotated. It does appear that the active response is "flatter" than the passive response and this is due in part to the (neoprene) moderation of the interrogating flux and the fact that the neutron generator is slightly asymmetric with respect to the vertical profile of the 200 liter drum since the counter must also accommodate 400 liter drums.

Upon examination of the sigma vectors in Table V through Table X we see a definite pattern with the diagonal elements of the sigma vectors as the radius is increased. The diagonal elements get "stronger" with respect to the off-diagonal elements for increasing radii. This is a direct result of the response of the counter which is now stored as a content addressable memory which can be retrieved and compared with the unknown assay. Associated with each diagonal element of each drum-matrix configuration is an NIT correction factor, CF_{KdP}, which is obtained from the database schema utilizing the volume weighted correction factors (Table IV) and minimized *KdP* (**Eq. 8**). This procedure is accomplished for both passive and active modes where separate NIT correction factors are applied.

The case for single point sources is trivial since we are essentially solving the identity matrix problem. A preliminary study, or campaign, of multi-point sources began as this paper was submitted. The active mode preliminary results are shown the combustibles matrix configured drum (ETG) using the ½ gram plutonium PIDIE standards PIDIE-1 (82 mg Pu-239 equivalent apparent mass), PIDIE-5 (77 mg Pu-239 equivalent apparent mass) and the 1 gram uranium standard EUREX-13 (259 mg Pu-239 equivalent apparent mass) in various frame positions as shown in Table XI and Table XII. The ratio value shown in the two tables is the ratio of the sum of the apparent mass to the volume weighted corrected measured mass (Pu-239 equivalent). The value $CF(KdP)_a$ is the "actual" *KdP* correction factor, *i.e.*, the value using the apparent mass weighted by the known source frame positions. The quantity $CF(Kdp)_m$ is the "minimized" *KdP* correction factor as obtained through **Eq. 8**. The gauge of the success of the KdP method is how well the "actual" and "minimized" *KdP* correction factors compare with the ratio.

The first two rows if data in Table XI shows the EUREX-13 and PIDIE-1 alone at (h2,r1). Both KdP methods predicted the expected correction factor for EUREX-13 but not so for the PIDIE-1. This was due to the fact that the frame position (*h1,r1*) had a nearly identical *KdP* assay value as (*h2,r1*) which has a correction factor of 1.702. The frame correction factor for ETG (*h2,r1*) is 1.057. The explanation for this was that the PIDIE-1 was placed slightly lower in the expected frame source position of (*h2,r1*). This is a testament of how sensitive the NIT technique is to source position and the limitation of simply choosing the minimized *KdP* with such a "coarse"

frame measurement database. The remaining rows of data in Table XI shows the two PIDIE sources moved about and, with only one exception, the minimized *KdP* correction factors "tracked" the ratio with one exception which is a direct result of the limitation of the current *KdP* method as described above.

The data in Table XII depicts three measurements representing three frame positions for the EUREX-13 standard while fixing the two PIDIE standards. In general the *KdP* correction factors agree with the ratios. Any discrepancies could be accounted for differences in active source-matrix coupling between the calibration and assay due to shifting of the mixed combustibles waste within the ETG configuration.

In the immediate future, the plan is to utilize the high-density wood (WHD) and neoprene (NEO) matrix configurations with similar mult-point source tests with, hopefully, larger mass plutonium standards (if possible). Such tests will better reveal the resolving power, success an limitations of the NIT minimized *KdP* technique. Perhaps the minimized *KdP* is not the best technique for NIT but maybe some sort of weighted scheme using the *KdP* values themselves. In addition, it may be advantageous to augment by measurement, or utilizing some interpolation scheme, the NIT database itself, and/or MCNP calculations.

Figure 6 Active assay door response for 200 L neoprene drum with Pu source at R=25.4 cm and H=42.5 cm.

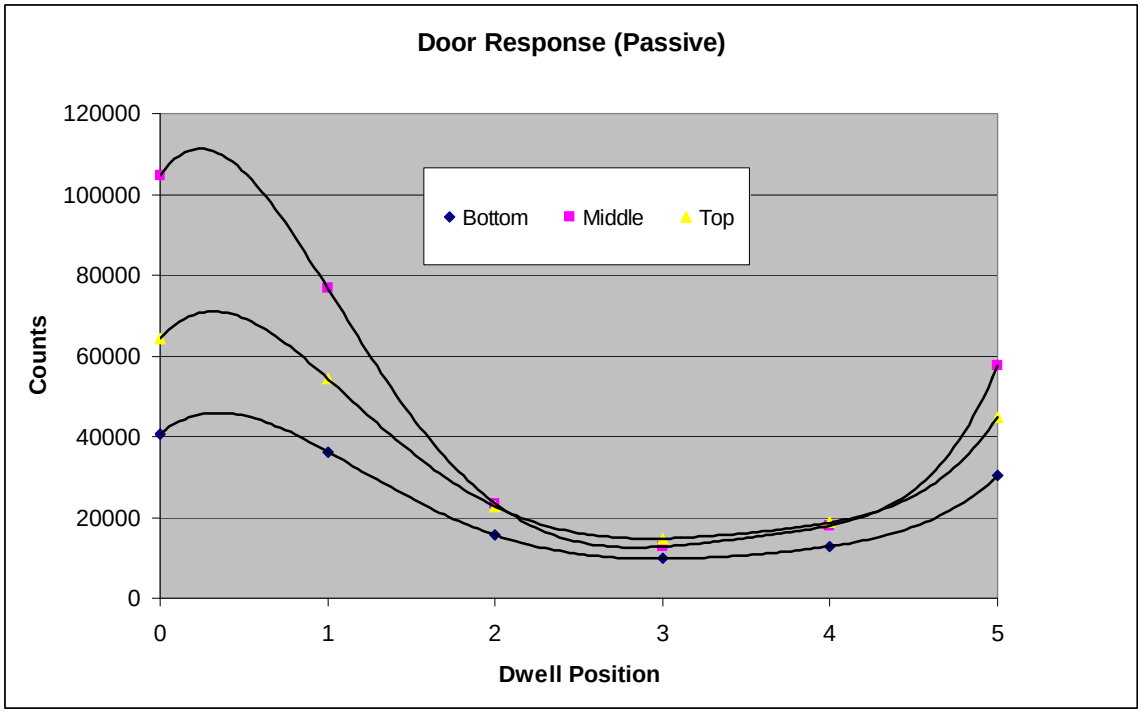

Figure 7 Passive assay door response for 200 L neoprene drum with Pu source at R=25.4 cm and H=42.5 cm.

Table V Passive sigma vectors for combustibles matrix.

Drum	Bottom	Middle	Top
ETG,h1,r1	0.004271	0.003683	0.002851
ETG,h2,r1	0.00172	0.006741	0.00756
ETG,h3,r1	0.003079	0.007412	0.00527
ETG,h1,r2	0.02285	0.017101	0.006589
ETG,h2,r2	0.016332	0.028642	0.022352
ETG,h3,r2	0.004467	0.020849	0.026543
ETG,h1,r3	0.054247	0.040398	0.015186
ETG,h2,r3	0.03415	0.056359	0.039007
ETG,h3,r3	0.020409	0.047076	0.053303
ETG,h1,r4	0.068666	0.053141	0.019198
ETG,h2,r4	0.043023	0.069777	0.043481
ETG,h3,r4	0.01956	0.055654	0.066642

Table VI Active sigma vector for combustibles matrix.

Drum	Bottom	Middle	Top
ETG,h1,r1	0.01104	0.011957	0.009908
ETG,h2,r1	0.010548	0.01104	0.011733
ETG,h3,r1	0.003727	0.006429	0.003878
ETG,h1,r2	0.020483	0.018397	0.016394
ETG,h2,r2	0.029284	0.032492	0.029437
ETG,h3,r2	0.01679	0.019784	0.023223
ETG,h1,r3	0.063501	0.06567	0.063449
ETG,h2,r3	0.059563	0.061648	0.058486
ETG,h3,r3	0.045719	0.049017	0.048748
ETG,h1,r4	0.077011	0.081381	0.078422
ETG,h2,r4	0.069066	0.072257	0.068496
ETG,h3,r4	0.055802	0.058406	0.060197

Table VII Passive sigma vectors for high-density wood matrix.

Drum	Bottom	Middle	Top
WHD,h1,r1	0.002135	0.002078	0.002733
WHD,h2,r1	0.003207	0.002575	0.003031
WHD,h3,r1	0.003746	0.002435	0.001786
WHD,h1,r2	0.050978	0.065703	0.04315
WHD,h2,r2	0.046622	0.066548	0.048183
WHD,h3,r2	0.02348	0.046118	0.045818
WHD,h1,r3	0.125962	0.128423	0.063188
WHD,h2,r3	0.107653	0.146952	0.111418
WHD,h3,r3	0.058171	0.117701	0.123425
WHD,h1,r4	0.148952	0.146216	0.078241
WHD,h2,r4	0.119747	0.160933	0.125204
WHD,h3,r4	0.0727	0.133411	0.144803

Table VIII Active sigma vectors for high-density wood matrix.

Drum	Bottom	Middle	Top
WHD,h1,r1	0.013092	0.022498	0.014623
WHD,h2,r1	0.012634	0.016025	0.008824
WHD,h3,r1	0.011234	0.01186	0.010084
WHD,h1,r2	0.019872	0.035007	0.0197
WHD,h2,r2	0.018641	0.033901	0.0172
WHD,h3,r2	0.010368	0.027113	0.020384
WHD,h1,r3	0.07365	0.088158	0.030548
WHD,h2,r3	0.052962	0.105505	0.04899
WHD,h3,r3	0.025529	0.076738	0.070096
WHD,h1,r4	0.110616	0.115736	0.074141
WHD,h2,r4	0.089012	0.133559	0.086902
WHD,h3,r4	0.065389	0.1037	0.109522

Table IX Passive sigma vectors for neoprene matrix.

Drum	Bottom	Middle	Top
NEO,h1,r1	0.001846	0.00144	0.002304
NEO,h2,r1	0.001773	0.002857	0.00305
NEO,h3,r1	0.002885	0.002452	0.001731
NEO,h1,r2	0.035008	0.03852	0.019561
NEO,h2,r2	0.031141	0.043593	0.034323
NEO,h3,r2	0.020267	0.035573	0.032901
NEO,h1,r3	0.102536	0.101315	0.050821
NEO,h2,r3	0.082876	0.115177	0.086142
NEO,h3,r3	0.048605	0.091695	0.094671
NEO,h1,r4	0.125944	0.122033	0.066691
NEO,h2,r4	0.097652	0.133538	0.102264
NEO,h3,r4	0.062964	0.109434	0.117999

Table X Active sigma vectors for neoprene matrix.

Drum	Bottom	Middle	Top
NEO,h1,r1	0.033827	0.153462	0.017707
NEO,h2,r1	†	†	†
NEO,h3,r1	0.013891	0.231006	0.032028
NEO,h1,r2	0.019426	0.105271	0.022974
NEO,h2,r2	0.011979	0.11679	0.024256
NEO,h3,r2	0.013695	0.066812	0.042546
NEO,h1,r3	0.045952	0.096092	0.045195
NEO,h2,r3	0.042517	0.064495	0.044947
NEO,h3,r3	0.021228	0.067311	0.04996
NEO,h1,r4	0.100085	0.109094	0.076915
NEO,h2,r4	0.087129	0.10841	0.088629
NEO,h3,r4	0.067949	0.104252	0.091392

†The data for (*h2,r1*) was not available.

Table XI Multi point source measurements performed with PIDIE-1, PIDIE-5 and EUREX-13 configured in several frame positions within the ETG drum.

Source1	Source2	Ratio	$CF(KdP)_a$	$CF(KdP)_m$
EUREX-13 (H2, R1)	N/A	1.060	1.057	1.057
PIDIE-1 (H2, R1)	N/A	0.977	1.057	1.702
PIDIE-1 (H2,R1)	PIDIE-5 (H2,R2)	1.046	1.076	1.057
PIDIE-1 (H2,R1)	PIDIE-5 (H2,R3)	1.009	0.982	1.092
PIDIE-1 (H2,R2)	PIDIE-5 (H2,R4)	1.009	0.968	1.092
PIDIE-1 (H2,R2)	PIDIE-5 (H1,R4)	1.203	1.147	1.092
PIDIE-1 (H2,R2)	PIDIE-5 (H3,R4)	0.968	0.948	0.898
PIDIE-1 (H1,R2)	PIDIE-5 (H3,R4)	1.219	1.271	1.092
PIDIE-1 (H3,R2)	PIDIE-5 (H1,R2)	1.295	1.403	0.898

Table XII Multi point source measurements performed with PIDIE-1 fixed at (h3,r2) and PIDIE-5 fixed at (h1,r2) and EUREX-13 moved to three frame positions within the ETG drum.

EUREX-13	Ratio	$CF(KdP)_a$	$CF(KdP)_m$
H1,R3	1.320	1.311	1.191
H2,R3	1.064	1.082	1.092
H3,R3	1.003	1.060	0.898

CONCLUSION

We have shown that the Neutron Imaging Technique (NIT) utilizing the minimized KdP method is a viable way of correcting for spatially non-uniform Special Nuclear Material (SNM) distributions within known matrix types of, generally, homogeneous manner for both passive and active neutron singles counting. The minimized KdP amounts to a content-addressable memory mapping between the assay and the NIT database patterns that produces the imaging correction

factors. The NIT database stores the calibration patterns in a manner that is retrieved utilizing the classical assay volume weighted matrix correction factors for both the passive and active modes.

By the identity relationship, the NIT is successful for single point source SNM mass distributions. The technique is promising for multi-point source distributions although more verification is required and algorithm refinements appear necessary.

The NIT promotes the proper characterization of unknown drummed waste specifically when considering the mass result reported with associated MDA's (Minimum Detectable Activities) and TMU's (Total Measurement Uncertainties).

FUTURE CONSIDERATIONS

During the NIT study it has been noted the following future considerations:

- Parameterize the interrogating background for each detector group; Currently, the algorithm takes the active interrogating background which is parameterized as the detector sum and divides by the number of detector banks. This can lead to pattern mismatching within some highly hydrogenous matrix types.

- Consider strong/weak multiple SNM distributions for verification.

- Utilize, or incorporate, neural networks which are much better designed to solve content addressable memory applications.

- Incorporate a "check-sum" between the passive and active modes in conjunction to the HRGS (High Resolution Gamma Spectrometry) results and isotopic information if available.

- Using coincidence for the passive mode in conjunction to the singles – this requires multiple coincidence analyzers or a list mode device with source tagging.

- Compare to the technique [7] that exploits the Doubles to Triples ratio as a means of correcting non-uniform SNM mass distributions.

- Augment the NIT database with either measurements or MCNP.

REFERENCES

1. Menlove, H.O., Baca, J., Miller, M.L., Harker, W.C., Kroncke, K.E., Takashi, S., et al., "WDAS Operation Manual Including the Add-a-Source Function," Los Alamos National Laboratory report LA-12292-M (April 1992).

2. Caldwell, J.T., et al., "The Los Alamos Second Generation System for Passive and Active Neutron Assay of Drum Size Containers", Los Alamos National Laboratory report, LA-10774-MS, UC15 (September 1986).

3. Wilkins, C.G., Alvarez, E., Croft, S., Villani, M.F., Ambrifi, A., Simone, G., “PANWAS: A Passive/Active Neutron Waste Assay System for the Radiological Characterization of Waste Packages at the Nucleco Facility at Casaccia,” WM’06, Tucson, Arizona, February 26-March 2, 2006.

4. J. T. Caldwell, *et al*, "Greatly Improved Transuranic Waste Accuracy Using Neutron Signal Imaging," Transactions on American Nuclear Society, Vol. 64, 202 (1991).

5. DISPIM®, BIL Solutions Catalog (www.bilsolutions.co.uk).

6. D.C. Hensley, “Source Imaging of Drums in the *AP**Nea* System,”, 4th Non-Destructive Assay and Non-Destructive Examination Waste Characterization Conference, Salt Lake City, Utah (October 24th, 1995).

7. H.O Menlove, *et al*, “SuperHENC: Final Performance and Certification Summary,” LAUR-01-6459, Environmental Management Nondestructive Assay Characterization Conference, Denver, Colorado, December 11-13, 2001.

8. C G Wilkins, E Alvarez, A Ambrifi, S Croft, G Simone, M F Villani, “Modifications to Improve the Measurement Uncertainty of a Passive/Active Neutron Waste Assay System,” INMM’06, Nashville, TN, July 16–20, 2006.